



1 **Ozone formation sensitivity study using machine learning**
2 **coupled with the reactivity of VOC species**

3 Junlei Zhan¹, Yongchun Liu^{1*}, Wei Ma¹, Xin Zhang², Xuezhong Wang², Fang Bi²,
4 Yujie Zhang², Zhenhai Wu², Hong Li^{2*}

5 1. Aerosol and Haze Laboratory, Advanced Innovation Center for Soft Matter Science
6 and Engineering, Beijing University of Chemical Technology, Beijing 100029, China

7 2. State Key Laboratory of Environmental Criteria and Risk Assessment, Chinese
8 Research Academy of Environmental Sciences, Beijing 100012, China

9 Correspondence: liuyc@buct.edu.cn; lihong@craes.org.cn



10 Abstract

11 The formation of ground-level ozone (O_3) is dependent on both atmospheric chemical
12 processes and meteorological factors. Traditional models have difficulty assessing O_3
13 formation sensitivity in a timely manner due to the limitations of flexibility and
14 computational efficiency. In this study, a random forest (RF) model coupled with the
15 reactivity of volatile organic compound (VOC) species was used to investigate the O_3
16 formation sensitivity in Beijing from 2014 to 2016, and evaluate the relative importance
17 (RI) of chemical and meteorological factors to O_3 formation. The results showed that
18 the O_3 prediction performance using initial concentrations of VOC species ($R^2 = 0.87$)
19 was better than that using total VOCs (TVOCs) concentrations ($R^2 = 0.77$). Meanwhile,
20 the RIs of VOC species correlated well with their O_3 formation potentials (OFPs). O_3
21 formation presented a negative response to NO_x , $PM_{2.5}$ and relative humidity, and a
22 positive response to temperature, solar radiation and VOCs. The O_3 isopleth curves
23 calculated by the RF model were generally comparable with those calculated by the
24 box model. O_3 formation shifted from a VOC-limited regime to a transition regime from
25 2014 to 2016. This study demonstrates that the RF model coupled with the initial
26 concentrations of VOC species could provide an accurate, flexible, and computationally
27 efficient approach for O_3 sensitivity analysis.



28 **1. Introduction**

29 Ground-level ozone (O_3) pollution, which can cause adverse human health effects
30 such as cardiovascular and respiratory diseases, has received increasing attention in
31 recent decades (Cohen et al., 2017). As important precursors of O_3 , volatile organic
32 compounds (VOCs) in the atmosphere are oxidized to produce peroxy radicals (RO_2)
33 and hydroperoxy radicals (HO_2), which will accelerate the $NO-O_3-NO_2$ cycle, thus
34 leading to the accumulation of O_3 (Wang et al., 2017a). The production and loss of RO_2
35 and HO_2 are highly dependent on the concentration ratio of VOCs and NO_x in the
36 atmosphere. Hence, atmospheric O_3 concentrations or production rates show a
37 nonlinear relationship with VOCs and NO_x . Moreover, the O_3 -VOC- NO_x sensitivity is
38 readily influenced by VOC species (Tan et al., 2018), meteorological parameters (Liu
39 et al., 2020a; Liu & Wang 2020), and even atmospheric particulate matter (Li et al.,
40 2019), thus, exhibits high temporal and spatial variability. Therefore, it is urgent to
41 develop an accurate and highly efficient method for timely assessing the sensitivity
42 regime of O_3 production and evaluating the effectiveness of a potential measure on O_3
43 pollution control.

44 The sensitivity of O_3 formation can usually be analysed using observed indicators,
45 such as ozone production efficiency (OPE, $\Delta O_3/\Delta NO_z$) (Wang et al., 2010; Lin et al.,
46 2011), $HCHO/NO_y$ (Martin et al., 2004), and H_2O_2/NO_z (or H_2O_2/HNO_3) (Sillman 1995;
47 Hammer et al., 2002; Wang et al., 2017a), observation-based model (OBM) (Vélez-
48 Pereira et al., 2021) and chemical transport models including community multiscale air



49 quality (CMAQ) (Djalalova et al., 2015) and Weather Research and Forecasting with
50 Chemistry (WRF-Chem) model (Wang et al., 2020a). The observed indicators can be
51 utilized to quickly diagnose the sensitivity regime of O₃ production. However, the
52 accuracy is sensitive to the precision of tracer measurements. In addition, this method
53 lacks the predictability of O₃ concentrations for policy-making. OBMs combine *in-situ*
54 field observations and chemical box models, which are built on widely-used chemistry
55 mechanisms (e.g., MCM, Carbon Bond, RACM or SAPRC), and applied to the
56 observed atmospheric conditions to simulate the *in-situ* O₃ production rate (Mo et al.,
57 2018). The sensitivity of O₃ production to various O₃ precursors, including NO_x and
58 VOCs can be diagnosed based on the empirical kinetic modeling approach (EKMA) or
59 quantitatively assessed with the relative incremental reactivity (RIR). Chemical
60 transport models, which are driven by meteorological dynamics and incorporated with
61 the emissions of pollutants and the complex atmospheric chemical mechanism, provide
62 a powerful tool for simulating various atmospheric processes, including spatial
63 distribution, regional transport vs. local formation, source apportionment and
64 production rates of pollutants and so on (Sayeed et al., 2021). At present, OBMs are
65 widely used to investigate O₃ formation sensitivity in China. Previous studies indicated
66 that O₃ formation in urban areas of China is located in a VOC-limited or a transition
67 regime and varies with time and location (Ou et al., 2016; Wang et al., 2017a; Zhan et
68 al., 2021).

69 Although both OBMs and chemical transport models can assess the sensitivity of



70 O₃ production and predict the O₃ pollution level in a scenario of control measures, the
71 calculation accuracy is affected by the uncertainty of input parameters (Tang et al., 2011;
72 Yang et al., 2021b). In addition, both of them are time-consuming and expensive when
73 computational resources are considered. Thus, they are mostly applied to sampling
74 cases with a short time span (days or weeks) (Xue et al., 2014; Ou et al., 2016), and
75 identifying O₃ formation sensitivity in a timely manner is difficult. Compared to
76 traditional methods, machine learning (ML) is able to capture the main factors affecting
77 atmospheric O₃ formation in a timely manner with great flexibility (without the
78 constraints of time and space) and high computational efficiency (Wang et al., 2020c;
79 Grange et al., 2021; Yang et al., 2021a). Recently, ML based on convolutional neural
80 network (CNN), random forest (RF) and artificial neural network (ANN) models has
81 been applied in simulating atmospheric O₃ and shown good performance in O₃
82 prediction (Ma et al., 2020; Xing et al., 2020). For example, Ma et al. (Ma et al., 2021a)
83 simulated O₃ concentrations in the Beijing-Tianjin-Hebei (BTH) region from 2010-
84 2017 using an RF model that considered meteorological variables and output variables
85 from chemical transport models, and the correlation coefficient (R^2) between the
86 observed and modelled O₃ concentrations was greater than 0.8. Liu et al. (Liu et al.,
87 2021) also reported a high accuracy (80.4%) for classifying pollution levels of O₃ and
88 PM_{2.5} at 1464 monitoring sites in China using an RF model. According to these previous
89 studies, the RF model has shown good performance in terms of prediction accuracy and
90 computational efficiency (Wang et al., 2016; Wang et al., 2017b).



91 However, many ML studies have used total VOCs (TVOCs) to simulate O₃
92 formation and rarely considered the effect of VOC species on O₃ formation sensitivity
93 (Feng et al., 2019; Liu et al., 2021; Ma et al., 2021a). Thus, they were unable to identify
94 the chemical reactivity of a single species to O₃ formation, which may lead to
95 underestimations or even misunderstandings of the role of VOCs in O₃ formation
96 because the same concentration of TVOCs with different compositions may lead to
97 different OPEs. In addition, VOCs react with OH radicals during atmospheric transport,
98 which is the most important sink of VOCs (Carlo et al., 2004; Liu et al., 2020b). Makar
99 et al. (Makar et al., 1999) reported that highly reactive species, such as isoprene, were
100 underestimated by 40% when the OH reactions were ignored. Other studies indicated
101 that the initial concentrations of VOCs, which account for the photochemical loss of
102 VOCs during transport, were more representative of pollution levels in the sampling
103 area than the observed VOCs (Yuan et al., 2013; Zhan et al., 2021). However, whether
104 the ML model can identify the connection between the reactivity of VOC species and
105 O₃ formation sensitivity has not been clarified.

106 In this study, we used the RF model to evaluate the prediction performance of
107 atmospheric O₃ using the TVOCs, measured VOC species and photochemical initial
108 concentration (PIC) of VOC species. We compared the relative importance (RI) of the
109 precursors (VOC species, NO_x, PM_{2.5}, CO) and the meteorological parameters
110 (temperature, solar radiation, relative humidity, wind speed and direction) on O₃
111 formation in the summer of Beijing from 2014 to 2016. We also discussed the



112 possibility of connecting the RIs of VOCs with their OFPs and the changes in O₃-VOC-
113 NO_x sensitivity based on the RF model from 2014 to 2016. Our study indicates that the
114 RF model combined with initial concentrations of VOC species can simulate O₃
115 concentrations well and provides a flexible and efficient tool for O₃ modelling in a near
116 real-time way.

117 **2. Methods**

118 **2.1 Sampling site and data**

119 The sampling site (40.04°N, 116.42°E) is located at the campus of Chinese
120 Research Academy of Environmental Sciences and was described in our previous work
121 (Zhang et al., 2021). Briefly, the station is located two kilometers from the north 4th ring
122 road and surrounded by a mixed residential and commercial area. The concentrations
123 of VOCs, NO_x, CO, O₃ and PM_{2.5} were measured at 8 m above ground level at this
124 location. Meteorological parameters, including temperature (T), relative humidity (RH),
125 wind speed and direction (WS&WD), solar radiation (SR), were monitored at 15 m
126 above ground level. VOCs were measured by an online commercial instrument (GC-
127 866, Chromatotec, France), which consisted of two independent analysers for detecting
128 C₂-C₆ and C₆-C₁₂ hydrocarbon components. More details about the observations can
129 be found in the Supplemental Materials (S1). The PICs of VOCs were calculated
130 according to the method reported in our previous work (Zhan et al., 2021) and the
131 Supplemental Materials (S2).

132 **2.2 Random forest model**

133 The random forest (RF) is a type of decision tree that can be used for classification



134 and regression (Breiman 2001). During the training process, the model creates a large
135 number of different decision trees with different sample sets at each node, and then
136 averages the scores of each decision tree as its final score to obtain more accurate results
137 that avoid large bias and overfitting (Breiman 2001). Approximately one-third of the
138 samples are excluded from the sample when the decision tree is built and used to
139 calculate the out-of-bag data error. Hence, RF can evaluate the RI of variables via out-
140 of-bag (OOB) data error (Svetnik et al., 2003),

$$141 \quad RI_i = \sum (\text{errOOB2}_i - \text{errOOB1}_i) / N \quad (1)$$

142 where N represents the number of decision trees, and errOOB1 and errOOB2 represent
143 the out-of-bag data error of feature i before and after adding tiny data noise (Kohavi &
144 John 1997; Breiman 2001), respectively. The RI_i reflects the response of the RF model
145 to feature i after adding tiny data noise. It was used to evaluate the importance and
146 sensitivity of feature i to O_3 formation in this study. More details about RI can be found
147 in the Supplemental Materials (S3). To verify the stability of the model, we interrupted
148 the continuity of the time series, fed the randomly arranged inputs to the model, and
149 performed a significance test on the RI. The results showed that there was no significant
150 difference among the different tests ($P > 0.05$, $R^2 > 0.97$).

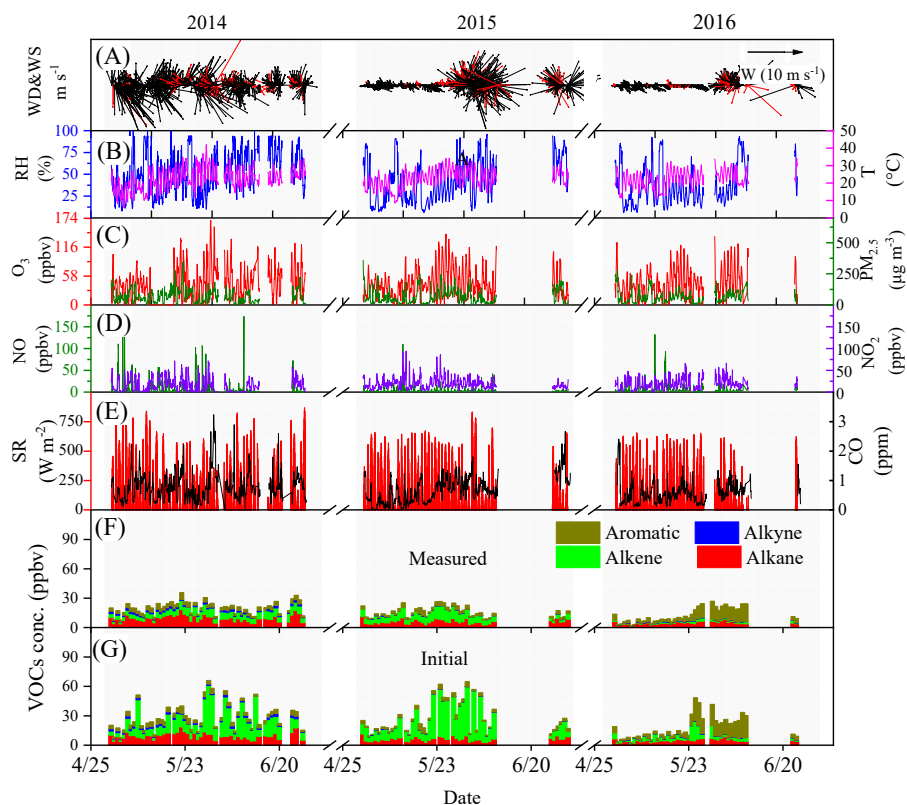
151 **3. Results and discussion**

152 **3.1 Overview of air pollutants and meteorological conditions**

153 Figure 1 shows the time series of air pollutants and meteorological parameters
154 during the observations from 2014 to 2016. In 2014, 2015 and 2016, the wind direction



155 was dominated by northwest winds (Figure S1), with mean wind speeds of 3.1 ± 2.7 m
156 s^{-1} , 2.3 ± 2.2 m s^{-1} , and 1.3 ± 1.2 m s^{-1} , respectively, and the mean daytime temperature
157 were 22.3 ± 5.8 , 23.9 ± 5.0 and 24.0 ± 4.4 °C, respectively. The average value of SR
158 decreased from 162.9 to 150.8 W m^{-2} during the observation period. As shown in Figure
159 1F-G, in 2014, 2015 and 2016, the mean VOC concentrations were 20.3 ± 10.9 , $15.8 \pm$
160 8.3 and 12.1 ± 7.7 ppbv, respectively, while the mean initial VOC concentrations were
161 28.1 ± 25.7 , 27.2 ± 32.6 and 16.4 ± 16.1 ppbv, respectively. Both the measured VOCs
162 and initial VOCs showed a decline along with a decrease in $PM_{2.5}$ concentration from
163 67.2 ± 53.5 to 61.1 ± 48.6 $\mu g m^{-3}$ due to the Air Pollution Prevention and Control Action
164 Plan in China (Zhao et al., 2021). However, O_3 concentrations showed a slight upward
165 trend from 38.7 ± 33.4 to 42.7 ± 27.9 ppbv from 2014 to 2015 and then to 44.0 ± 29.6
166 ppbv in 2016. A similar trend was observed for NO_x concentrations (Figure S2). As
167 shown in Figure 1F-G, the concentrations of four types (alkanes, alkenes, alkynes, and
168 aromatics) of VOCs showed significant differences from 2014 to 2016 due to the
169 variations in emission sources (Zhang et al., 2021). In addition to VOC species, the
170 variations in other parameters, such as meteorological conditions and $PM_{2.5}$, should
171 have a complex influence on O_3 -VOC- NO_x sensitivity (Li et al., 2019; Ma et al., 2021b).



172

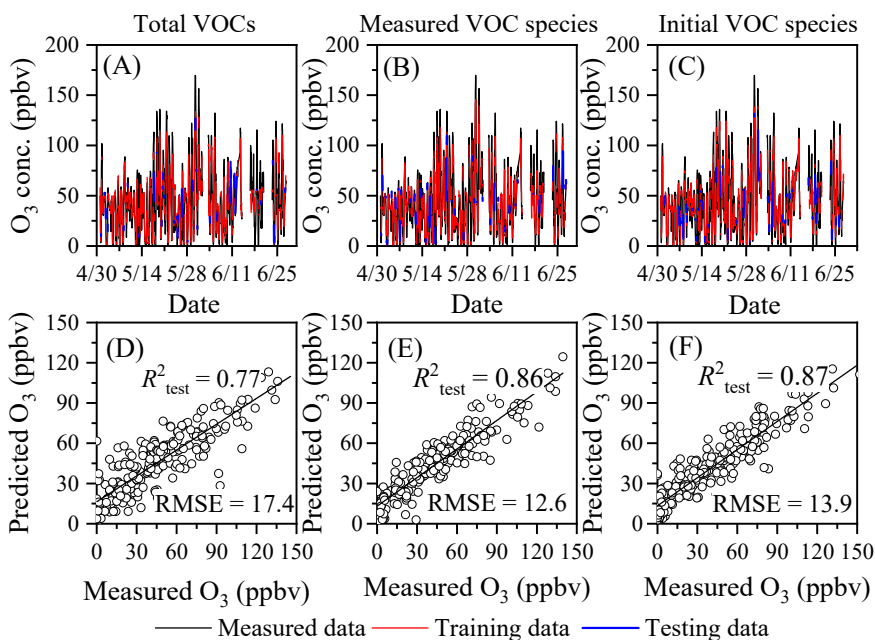
173 **Figure 1.** Time series of air pollutants and meteorological parameters during
174 observations in Beijing.

175 3.2 Prediction performance of the model.

176 To build a robust model, we evaluated the prediction performance of the RF model
177 for the ambient O₃ simulation. Figure 2 shows the O₃ prediction performance when
178 chemical species (including VOCs, NO_x, PM_{2.5}, CO) and meteorological factors (i.e.,
179 WS, WD, SR, T and RH) were used as inputs in the RF model. The details of the
180 modelling and input parameters are shown in Table S1. Figure 2A-C shows the time
181 series of the measured and modelled O₃ concentrations, which were simulated using



182 the TVOCs, measured VOC species and initial VOC species as input variables along
183 with the same set of other parameters. The correlation coefficients (R^2) of the training
184 data were 0.88, 0.94 and 0.94 for the TVOCs, measured VOC species and initial VOC
185 species, respectively. The corresponding root mean squared errors (RMSEs) for the
186 predicted O_3 concentrations were 9.9, 9.3 and 9.1. Figure 2D-F shows the prediction
187 performance of the testing dataset under these three circumstances. When the TVOCs
188 were split into VOC species, the R^2 increased from 0.77 to 0.86 as the number of data
189 features increased. Therefore, the VOC composition has a significant influence on O_3
190 prediction using the RF model. Thus, our model has good prediction performance (R^2
191 = 0.87) when combined with the initial VOC species. In previous studies using TVOCs,
192 the influence of VOC composition was neglected (Liu et al., 2021; Ma et al., 2021a).
193 Therefore, our results indicate that the RF model can accurately predict O_3
194 concentrations when the concentrations of VOC species are considered and identify the
195 connection between the reactivity of VOC species and O_3 formation in the atmosphere.



196

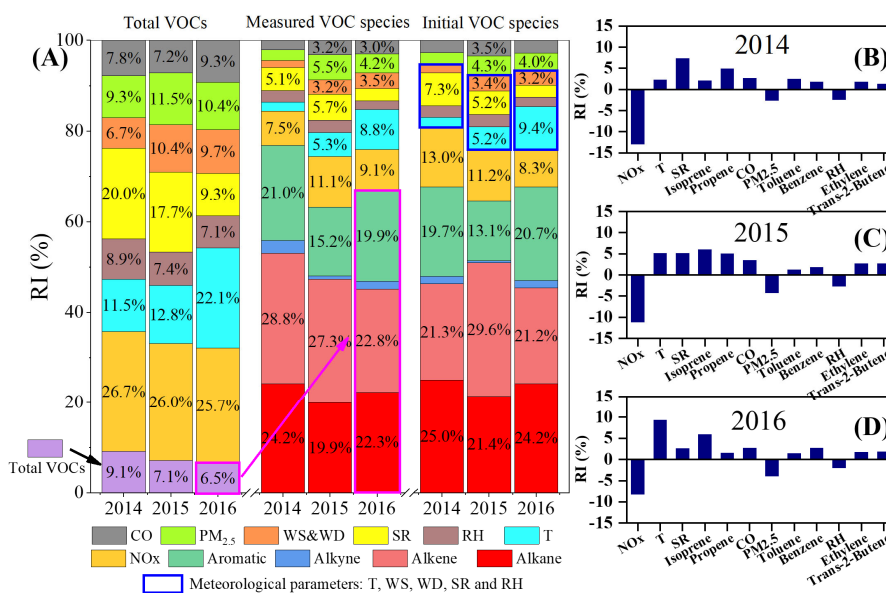
197 **Figure 2.** Comparison of the predicted and measured O₃ concentrations in Beijing in
198 the summer of 2014. (A and D: TVOC concentrations; B and E: measured
199 concentrations of VOC species; C and F: initial concentrations of VOC species)

200 3.3 Relative importance of major factors

201 Figure 3A shows the RIs of different ambient factors, including chemical and
202 meteorological variables on O₃ formation. The difference in the RIs is also compared
203 using the TVOCs and the VOC species as inputs. Chemical factors (including VOC
204 species, NO_x, PM_{2.5} and CO) accounted for 83.1% of the contribution to O₃ production
205 in the summer of 2016. Meanwhile, VOC species accounted for approximately 66.7%
206 of O₃ production while the RIs using TVOC concentrations accounted for only 6.5%.
207 Ma et al. (Ma et al., 2021b) analysed the contribution of meteorological conditions and
208 chemical factors to O₃ formation on the North China Plain (NCP) using the CMAQ



209 model in combination with process analysis and found that chemical factors dominate
 210 O₃ formation in summer. Using probability theory, Ueno et al. (Ueno & Tsunematsu
 211 2019) also found that VOCs/NO_x dominate O₃ production compared to meteorological
 212 variables. Thus, our results are similar to those of previous studies based on chemical
 213 models (Ueno & Tsunematsu 2019; Ma et al., 2021b), which demonstrates that the RF
 214 model can reflect the contribution of VOC species to O₃ production even if the observed
 215 VOC species are used.



216
 217 **Figure 3.** Percentage of RI for O₃ precursors and meteorological parameters (A) and
 218 the top 12 factors with high values of RI in 2014-2016 (B-D: using initial concentrations
 219 of VOC species).

220 Although ML is widely used to understand air pollution, explanations of ML
 221 results (e.g., RI) are somewhat vague because ML is a black-box model (Sayeed et al.,
 222 2021). Here, we compared the RIs of VOCs calculated using the initial VOC species



223 and the observed VOC species with the O₃ formation potentials (OFPs). The OFPs were
224 calculated by the maximum incremental reactivity (MIR) method (Carter 2010). As
225 shown in Figure S3, the RIs showed good correlations with the OFP. Interestingly, the
226 initial concentrations of VOC species improved the correlation coefficients between the
227 RIs and OFPs. Furthermore, we calculated the RIs and OFPs of different species using
228 the observed data during the campaign study in Daxing District in the summer of 2019
229 (Zhan et al., 2021), and a strong correlation was observed between the RIs of the initial
230 VOC species and the OFPs (Figure S4). These results indicate that the RIs of the initial
231 VOCs species in the ML model should partially reflect the chemical reactivity of VOCs
232 to produce O₃ in the atmosphere.

233 Although the RIs calculated using the initial VOC species slightly changed
234 compared to those calculated using the observed VOCs (Table S2), VOCs still
235 dominated O₃ formation (Figure 3A). For example, the initial VOCs dominated O₃
236 production in 2014, 2015, and 2016, with RI values of 67.7, 64.5 and 67.7%
237 respectively. Li et al. (Li et al., 2020a) used a multiple linear regression (MLR) model
238 to study the contribution of anthropogenic and meteorological factors to O₃ formation
239 in China from 2013-2019 and found that meteorological factors accounted for 36.8%
240 and anthropogenic factors accounted for 63.2%, which is similar to our results. Figure
241 3B-D shows the top 12 factors having a strongly influence on O₃ production.
242 Interestingly, NO_x, PM_{2.5} and RH showed negative responses to O₃ formation, while
243 other variables, including T, SR, CO and all of the VOCs, showed positive responses.



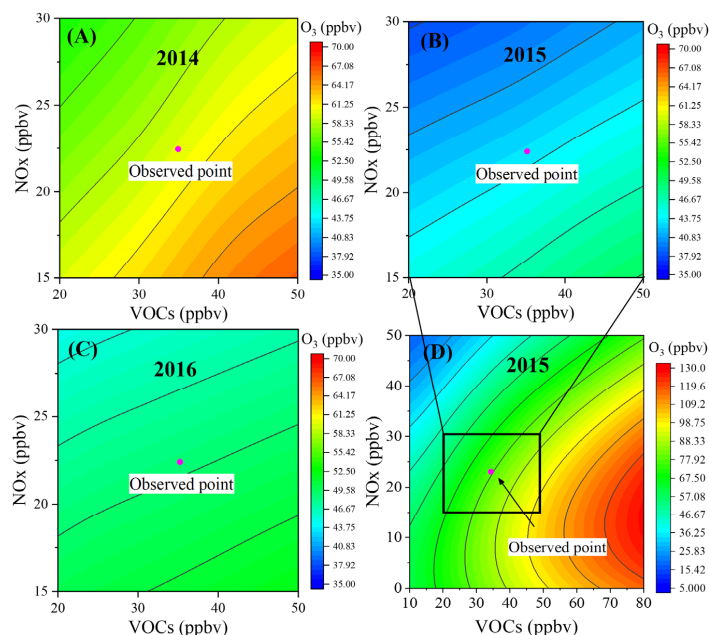
244 Thus, a decrease in NO_x, PM_{2.5} or RH will lead to an increase in O₃ concentration while
245 a decrease in T, SR, CO and VOCs will lead to a decrease in O₃ concentration. Although
246 O₃ formation is highly related to the photolysis of NO₂, a previous study demonstrated
247 that it is VOC-limited in summer in Beijing (Zhan et al., 2021). This finding is
248 consistent with the observed negative response of O₃ to NO_x in this work. High
249 concentrations of PM_{2.5} can reduce solar radiation and increase the sinks of reactive
250 radicals (HO_x and RO_x) (Li et al., 2019). In addition, high RH usually coincides with
251 low surface O₃ concentrations in field observations, which can be ascribed to the
252 inhibition of O₃ formation by the transfer of NO₂/ONO₂-containing products into the
253 particle phase and the promotion of dry deposition of O₃ on the surface (Kavassalis &
254 Murphy 2017; Yu 2019). These previous works can well explain the observed negative
255 response of O₃ to PM_{2.5} and RH in Figure 3B. Previous studies have observed a positive
256 correlation between the O₃ concentration and T or SR (Steiner et al., 2010; Paraschiv
257 et al., 2020; Li et al., 2021). Temperature can directly affect the chemical reaction rate
258 of O₃ formation (Fu et al., 2015), and SR can promote the photolysis of NO₂ (Hu et al.,
259 2017; Wang et al., 2020b), thus accelerating O₃ formation. As mentioned above, O₃
260 formation is VOC-limited in Beijing; thus, a positive response of O₃ concentration to
261 VOCs is observed in Figure 3B. Interestingly, the RIs of isoprene showed an increasing
262 trend from 2014 to 2016 because of the obvious reduction in anthropogenic VOCs
263 (Figure 1) (Zhang et al., 2021). In the context of global warming, studies should focus
264 on the factors that affect O₃ formation, including biogenic emissions, T and SR. Thus,



265 additional efforts will be required to reduce anthropogenic pollutants in the future.

266 **3.4 Ozone formation sensitivity**

267 To further analyse the sensitivity of O₃ to VOCs and NO_x from 2014 to 2016, we
268 plotted sensitivity curves for O₃ generation using the RF model, and the results are
269 shown in Figure 4A-C. Moreover, EKMA curves in 2015 were also obtained using the
270 OBM (Figure 4D). As shown in Figure 4A-C, O₃ formation was sensitive to VOCs in
271 the summer of Beijing during our observations, which is consistent with previous
272 studies that used box models (Li et al., 2020b) and chemical transport models (Shao et
273 al., 2021). This result is also consistent with the RIs of VOCs or NO_x to O₃ formation
274 (Figure 3B). Interestingly, the O₃ formation sensitivity to VOCs decreases or gradually
275 shifts from the observed point to the transition regime from 2014 to 2016 (Figure 4A-
276 C), which is similar to that reported by Zhang et al. (Zhang et al., 2021). These
277 phenomena can be ascribed to the increased importance of meteorological factors, such
278 as T, SR, and RH, for O₃ formation and the variation in anthropogenic VOC emissions
279 (Steiner et al., 2010; Ma et al., 2021b).



280

281 **Figure 4.** Ozone formation sensitivity curves from 2014–2016. (A, B, C: calculated by
282 the RF model for 2014, 2015, and 2016, respectively. D: calculated by the OBM for
283 2015)

284 We compared O₃ sensitivity using the RF model based on the TVOCs and the
285 initial VOC species in 2015. As shown in Figure S5, the O₃ concentrations predicted
286 using the initial concentrations of VOC species were more accurate after correcting the
287 reactivity during transport than those predicted using the TVOCs. Hence, a combination
288 of the RF model and initial VOCs species (Figure 4B) can accurately depict the
289 sensitivity regime of O₃ formation in comparison to the box model (Figure 4D),
290 although a difference is observable between the predicted O₃ concentrations using these
291 two models. In the box model, the O₃ isopleth plot was drawn with the maximum O₃
292 concentrations, while in the RF model, this plot was drawn with the real O₃



293 concentrations.

294 **4. Conclusions**

295 In summary, this work investigated O₃ formation sensitivity in the summer from
296 2014-2016 in Beijing using the RF model coupled with the reactivity of VOC species.
297 The results show that the prediction performance of O₃ by the RF model was
298 significantly improved when VOC species were considered compared to TVOCs.
299 Furthermore, after the photochemical loss of VOC species during transport was
300 corrected, the RIs of the VOC species were well correlated with the OFPs of VOC
301 species calculated using the MIR method, thus indicating that the RIs in the ML model
302 reflect the chemical reactivity of VOCs. Meanwhile, both NO_x and highly reactive
303 species (such as isoprene, propene, benzene, and toluene) played an important role in
304 O₃ formation. An increased contribution of temperature to O₃ production was observed,
305 which implied the importance of temperature to O₃ pollution in the context of global
306 warming conditions. Both the RF model and the box model results showed that O₃
307 formation was sensitive to VOCs in Beijing, although the sensitivity regime shifted
308 from VOC-limited regime to a transition regime from 2014 to 2016. Due to the high
309 computational efficiency of ML, the O₃ formation sensitivity plotted by the RF model
310 coupled with the reactivity of VOC species can provide an accurate, flexible and
311 efficient approach for analysing O₃ sensitivity in a near real-time way.

312

313 **Code and data availability**



314 The code and datasets of VOCs and meteorology are available and will be provided by
315 the corresponding authors Yongchun Liu (liuyc@buct.edu.cn) and Hong Li
316 (lihong@craes.org.cn) upon request. The solar radiation data are publicly available via
317 www.copernicus.eu/en.

318 **Supplement**

319 Supplementary information is available for this paper.

320 **Author contributions**

321 Junlei Zhan designed the idea and wrote this manuscript; Yongchun Liu and Hong Li
322 provided useful advice and revised the manuscript; Wei Ma performed box model
323 simulations; and Xin Zhang, Xuezhong Wang, Fang Bi, Yujie Zhang and Zhenhai Wu
324 conducted the campaign and compiled the data. All authors contributed to the
325 discussion of the results and writing of the manuscript.

326 **Competing interest**

327 The authors declare that they have no conflict of interest.

328 **Acknowledgments**

329 This research was financially supported by the Ministry of Science and Technology of
330 the People's Republic of China (2019YFC0214701), the National Natural Science
331 Foundation of China (41877306 and 92044301) and the programs from Beijing
332 Municipal Science & Technology Commission (No. Z181100005418015). We thank
333 Yizhen Chen for providing the meteorological parameter data for campaign studies.

334



335 **References**

- 336 Breiman, L. Random Forests. *Machine Learning*, 45, 5-32, 10.1023/A:1010933404324, 2001.
- 337 Carlo, P.D., Brune, W.H., Martinez, M., Harder, H., Leshner, R., Ren, X., Thornberry, T., Carroll,
338 M.A., Young, V., Shepson, P.B., Riemer, D., Apel, E., Campbell, C. Missing OH Reactivity
339 in a Forest: Evidence for Unknown Reactive Biogenic VOCs. *Science*, 304, 722-725,
340 doi:10.1126/science.1094392, 2004.
- 341 Carter, W. Updated maximum incremental reactivity scale and hydrocarbon bin reactivities for
342 regulatory applications. *California Air Resources Board Contract*, 1, 07-339, 2010.
- 343 Cohen, A.J., Brauer, M., Burnett, R., Anderson, H.R., Frostad, J., Estep, K., Balakrishnan, K.,
344 Brunekreef, B., Dandona, L., Dandona, R., Feigin, V., Freedman, G., Hubbell, B., Jobling,
345 A., Kan, H., Knibbs, L., Liu, Y., Martin, R., Morawska, L., Pope, C.A., Shin, H., Straif, K.,
346 Shaddick, G., Thomas, M., van Dingenen, R., van Donkelaar, A., Vos, T., Murray, C.J.L.,
347 Forouzanfar, M.H. Estimates and 25-year trends of the global burden of disease attributable
348 to ambient air pollution: an analysis of data from the Global Burden of Diseases Study 2015.
349 *The Lancet*, 389, 1907-1918, [https://doi.org/10.1016/S0140-6736\(17\)30505-6](https://doi.org/10.1016/S0140-6736(17)30505-6), 2017.
- 350 Djalalova, I., Delle Monache, L., Wilczak, J. PM_{2.5} analog forecast and Kalman filter post-
351 processing for the Community Multiscale Air Quality (CMAQ) model. *Atmospheric*
352 *Environment*, 108, 76-87, <https://doi.org/10.1016/j.atmosenv.2015.02.021>, 2015.
- 353 Feng, R., Zheng, H. J., Gao, H., Zhang, A. R., Huang, C., Zhang, J. X., Luo, K., Fan, J. R. Recurrent
354 Neural Network and random forest for analysis and accurate forecast of atmospheric
355 pollutants: A case study in Hangzhou, China. *J. Clean. Prod.*, 231, 1005-1015,
356 <https://doi.org/10.1016/j.jclepro.2019.05.319>, 2019.
- 357 Fu, T.-M., Zheng, Y., Paulot, F., Mao, J., Yantosca, R.M. Positive but variable sensitivity of August
358 surface ozone to large-scale warming in the southeast United States. *Nat. Clim. Change*, 5,
359 454-458, 10.1038/nclimate2567, 2015.
- 360 Grange, S.K., Lee, J.D., Drysdale, W.S., Lewis, A.C., Hueglin, C., Emmenegger, L., Carslaw, D.C.
361 COVID-19 lockdowns highlight a risk of increasing ozone pollution in European urban
362 areas. *Atmos. Chem. Phys.*, 21, 4169-4185, 10.5194/acp-21-4169-2021, 2021.
- 363 Hammer, M.-U., Vogel, B., Vogel, H. Findings on H₂O₂/HNO₃ as an indicator of ozone sensitivity
364 in Baden-Württemberg, Berlin-Brandenburg, and the Po valley based on numerical
365 simulations. *J. Geophys. Res. Atmos.*, 107, LOP 3-1-LOP 3-18,
366 <https://doi.org/10.1029/2000JD000211>, 2002.
- 367 Hu, B., Zhao, X., Liu, H., Liu, Z., Song, T., Wang, Y., Tang, L., Xia, X., Tang, G., Ji, D., Wen, T.,
368 Wang, L., Sun, Y., Xin, J. Quantification of the impact of aerosol on broadband solar
369 radiation in North China. *Sci. Rep.*, 7, 44851, 10.1038/srep44851, 2017.
- 370 Kavassalis, S.C., Murphy, J.G. Understanding ozone-meteorology correlations: A role for dry
371 deposition. *Geophys. Res. Lett.*, 44, 2922-2931, <https://doi.org/10.1002/2016GL071791>,
372 2017.
- 373 Kohavi, R., John, G.H. Wrappers for feature subset selection. *Artif. Intell.*, 97, 273-324,
374 [https://doi.org/10.1016/S0004-3702\(97\)00043-X](https://doi.org/10.1016/S0004-3702(97)00043-X), 1997.
- 375 Li, J., Cai, J., Zhang, M., Liu, H., Han, X., Cai, X., Xu, Y. Model analysis of meteorology and
376 emission impacts on springtime surface ozone in Shandong. *Sci. Total Environ.*, 771,



- 377 144784, <https://doi.org/10.1016/j.scitotenv.2020.144784>, 2021.
- 378 Li, K., Jacob, D.J., Liao, H., Zhu, J., Shah, V., Shen, L., Bates, K.H., Zhang, Q., Zhai, S. A two-
379 pollutant strategy for improving ozone and particulate air quality in China. *Nat. Geosci.*,
380 12, 906-910, [10.1038/s41561-019-0464-x](https://doi.org/10.1038/s41561-019-0464-x), 2019.
- 381 Li, K., Jacob, D.J., Shen, L., Lu, X., De Smedt, I., Liao, H. Increases in surface ozone pollution in
382 China from 2013 to 2019: anthropogenic and meteorological influences. *Atmos. Chem.*
383 *Phys.*, 20, 11423-11433, [10.5194/acp-20-11423-2020](https://doi.org/10.5194/acp-20-11423-2020), 2020a.
- 384 Li, Q., Su, G., Li, C., Liu, P., Zhao, X., Zhang, C., Sun, X., Mu, Y., Wu, M., Wang, Q., Sun, B. An
385 investigation into the role of VOCs in SOA and ozone production in Beijing, China. *Sci.*
386 *Total Environ.*, 720, 137536, <https://doi.org/10.1016/j.scitotenv.2020.137536>, 2020b.
- 387 Lin, W., Xu, X., Ge, B., Liu, X. Gaseous pollutants in Beijing urban area during the heating period
388 2007–2008: variability, sources, meteorological, and chemical impacts. *Atmos. Chem.*
389 *Phys.*, 11, 8157-8170, [10.5194/acp-11-8157-2011](https://doi.org/10.5194/acp-11-8157-2011), 2011.
- 390 Liu, H., Liu, J., Liu, Y., Ouyang, B., Xiang, S., Yi, K., Tao, S. Analysis of wintertime O₃ variability
391 using a random forest model and high-frequency observations in Zhangjiakou—an area
392 with background pollution level of the North China Plain. *Environ. Pollut.*, 262, 114191,
393 <https://doi.org/10.1016/j.envpol.2020.114191>, 2020a.
- 394 Liu, Y., Cheng, Z., Liu, S., Tan, Y., Yuan, T., Yu, X., Shen, Z. Quantitative structure activity
395 relationship (QSAR) modelling of the degradability rate constant of volatile organic
396 compounds (VOCs) by OH radicals in atmosphere. *Sci. Total Environ.*, 729, 138871,
397 <https://doi.org/10.1016/j.scitotenv.2020.138871>, 2020b.
- 398 Liu, Y., Wang, T. Worsening urban ozone pollution in China from 2013 to 2017 – Part 1: The
399 complex and varying roles of meteorology. *Atmos. Chem. Phys.*, 20, 6305-6321,
400 [10.5194/acp-20-6305-2020](https://doi.org/10.5194/acp-20-6305-2020), 2020.
- 401 Liu, Z., Qi, Z., Ni, X., Dong, M., Ma, M., Xue, W., Zhang, Q., Wang, J. How to apply O₃ and PM_{2.5}
402 collaborative control to practical management in China: A study based on meta-analysis
403 and machine learning. *Sci. Total Environ.*, 772, 145392,
404 <https://doi.org/10.1016/j.scitotenv.2021.145392>, 2021.
- 405 Ma, R., Ban, J., Wang, Q., Li, T. Statistical spatial-temporal modeling of ambient ozone exposure
406 for environmental epidemiology studies: A review. *Sci. Total Environ.*, 701, 134463,
407 <https://doi.org/10.1016/j.scitotenv.2019.134463>, 2020.
- 408 Ma, R., Ban, J., Wang, Q., Zhang, Y., Yang, Y., He, M.Z., Li, S., Shi, W., Li, T. Random forest model
409 based fine scale spatiotemporal O₃ trends in the Beijing-Tianjin-Hebei region in China,
410 2010 to 2017. *Environ. Pollut.*, 276, 116635, <https://doi.org/10.1016/j.envpol.2021.116635>,
411 2021a.
- 412 Ma, S., Shao, M., Zhang, Y., Dai, Q., Xie, M. Sensitivity of PM_{2.5} and O₃ pollution episodes to
413 meteorological factors over the North China Plain. *Sci. Total Environ.*, 792, 148474,
414 <https://doi.org/10.1016/j.scitotenv.2021.148474>, 2021b.
- 415 Makar, P.A., Fuentes, J.D., Wang, D., Staebler, R.M., Wiebe, H.A. Chemical processing of biogenic
416 hydrocarbons within and above a temperate deciduous forest. *J. Geophys. Res. Atmos.*, 104,
417 3581-3603, <https://doi.org/10.1029/1998JD100065>, 1999.
- 418 Martin, R.V., Fiore, A.M., Van Donkelaar, A. Space-based diagnosis of surface ozone sensitivity to



- 419 anthropogenic emissions. *Geophys. Res. Lett.*, 31, <https://doi.org/10.1029/2004GL019416>,
420 2004.
- 421 Mo, Z., Shao, M., Liu, Y., Xiang, Y., Wang, M., Lu, S., Ou, J., Zheng, J., Li, M., Zhang, Q., Wang,
422 X., Zhong, L. Species-specified VOC emissions derived from a gridded study in the Pearl
423 River Delta, China. *Sci. Rep.*, 8, 2963, [10.1038/s41598-018-21296-y](https://doi.org/10.1038/s41598-018-21296-y), 2018.
- 424 Ou, J., Yuan, Z., Zheng, J., Huang, Z., Shao, M., Li, Z., Huang, X., Guo, H., Louie, P.K.K. Ambient
425 Ozone Control in a Photochemically Active Region: Short-Term Despiking or Long-Term
426 Attainment? *Environ. Sci. Technol.*, 50, 5720-5728, [10.1021/acs.est.6b00345](https://doi.org/10.1021/acs.est.6b00345), 2016.
- 427 Paraschiv, S., Barbuta-Misu, N., Paraschiv, S.L. Influence of NO₂, NO and meteorological
428 conditions on the tropospheric O₃ concentration at an industrial station. *Energy Rep.*, 6,
429 231-236, <https://doi.org/10.1016/j.egy.2020.11.263>, 2020.
- 430 Sayeed, A., Choi, Y., Eslami, E., Jung, J., Lops, Y., Salman, A.K., Lee, J.-B., Park, H.-J., Choi, M.-
431 H. A novel CMAQ-CNN hybrid model to forecast hourly surface-ozone concentrations 14
432 days in advance. *Sci. Rep.*, 11, 10891, [10.1038/s41598-021-90446-6](https://doi.org/10.1038/s41598-021-90446-6), 2021.
- 433 Shao, M., Wang, W., Yuan, B., Parrish, D.D., Li, X., Lu, K., Wu, L., Wang, X., Mo, Z., Yang, S.,
434 Peng, Y., Kuang, Y., Chen, W., Hu, M., Zeng, L., Su, H., Cheng, Y., Zheng, J., Zhang, Y.
435 Quantifying the role of PM_{2.5} dropping in variations of ground-level ozone: Inter-
436 comparison between Beijing and Los Angeles. *Sci. Total Environ.*, 788, 147712,
437 <https://doi.org/10.1016/j.scitotenv.2021.147712>, 2021.
- 438 Sillman, S. The use of NO_y, H₂O₂, and HNO₃ as indicators for ozone-NO_x-hydrocarbon sensitivity
439 in urban locations. *J. Geophys. Res. Atmos.*, 100, 14175-14188,
440 <https://doi.org/10.1029/94JD02953>, 1995.
- 441 Steiner, A.L., Davis, A.J., Sillman, S., Owen, R.C., Michalak, A.M., Fiore, A.M. Observed
442 suppression of ozone formation at extremely high temperatures due to chemical and
443 biophysical feedbacks. *P. Natl. Acad. Sci. USA*, 107, 19685-19690,
444 [10.1073/pnas.1008336107](https://doi.org/10.1073/pnas.1008336107), 2010.
- 445 Svetnik, V., Liaw, A., Tong, C., Culberson, J.C., Sheridan, R.P., Feuston, B.P. Random Forest: A
446 Classification and Regression Tool for Compound Classification and QSAR Modeling. *J.*
447 *Chem. Inf. Comput. Sci.*, 43, 1947-1958, [10.1021/ci034160g](https://doi.org/10.1021/ci034160g), 2003.
- 448 Tan, Z., Lu, K., Jiang, M., Su, R., Dong, H., Zeng, L., Xie, S., Tan, Q., Zhang, Y. Exploring ozone
449 pollution in Chengdu, southwestern China: A case study from radical chemistry to O₃-
450 VOC-NO_x sensitivity. *Sci. Total Environ.*, 636, 775-786,
451 <https://doi.org/10.1016/j.scitotenv.2018.04.286>, 2018.
- 452 Tang, X., Zhu, J., Wang, Z.F., Gbaguidi, A. Improvement of ozone forecast over Beijing based on
453 ensemble Kalman filter with simultaneous adjustment of initial conditions and emissions.
454 *Atmos. Chem. Phys.*, 11, 12901-12916, [10.5194/acp-11-12901-2011](https://doi.org/10.5194/acp-11-12901-2011), 2011.
- 455 Ueno, H., Tsunematsu, N. Sensitivity of ozone production to increasing temperature and reduction
456 of precursors estimated from observation data. *Atmos. Environ.*, 214, 116818,
457 <https://doi.org/10.1016/j.atmosenv.2019.116818>, 2019.
- 458 Vélez-Pereira, A.M., De Linares, C., Belmonte, J. Aerobiological modeling I: A review of predictive
459 models. *Sci. Total Environ.*, 795, 148783, <https://doi.org/10.1016/j.scitotenv.2021.148783>,
460 2021.



- 461 Wang, P., Qiao, X., Zhang, H. Modeling PM_{2.5} and O₃ with aerosol feedbacks using WRF/Chem
462 over the Sichuan Basin, southwestern China. *Chemosphere*, 254, 126735,
463 <https://doi.org/10.1016/j.chemosphere.2020.126735>, 2020a.
- 464 Wang, T., Nie, W., Gao, J., Xue, L.K., Gao, X.M., Wang, X.F., Qiu, J., Poon, C.N., Meinardi, S.,
465 Blake, D., Wang, S.L., Ding, A.J., Chai, F.H., Zhang, Q.Z., Wang, W.X. Air quality during
466 the 2008 Beijing Olympics: secondary pollutants and regional impact. *Atmos. Chem. Phys.*,
467 10, 7603-7615, 10.5194/acp-10-7603-2010, 2010.
- 468 Wang, T., Xue, L., Brimblecombe, P., Lam, Y.F., Li, L., Zhang, L. Ozone pollution in China: A
469 review of concentrations, meteorological influences, chemical precursors, and effects. *Sci.*
470 *Total Environ.*, 575, 1582-1596, <https://doi.org/10.1016/j.scitotenv.2016.10.081>, 2017a.
- 471 Wang, Y., Gao, W., Wang, S., Song, T., Gong, Z., Ji, D., Wang, L., Liu, Z., Tang, G., Huo, Y., Tian,
472 S., Li, J., Li, M., Yang, Y., Chu, B., Petäjä, T., Kerminen, V.-M., He, H., Hao, J., Kulmala,
473 M., Wang, Y., Zhang, Y. Contrasting trends of PM_{2.5} and surface-ozone concentrations in
474 China from 2013 to 2017. *Natl. Sci. Rev.*, 7, 1331-1339, 10.1093/nsr/nwaa032, 2020b.
- 475 Wang, Y., Li, Y., Pu, W., Wen, K., Shugart, Y.Y., Xiong, M., Jin, L. Random Bits Forest: a Strong
476 Classifier/Regressor for Big Data. *Sci. Rep.*, 6, 30086, 10.1038/srep30086, 2016.
- 477 Wang, Y., Wen, Y., Wang, Y., Zhang, S., Zhang, K.M., Zheng, H., Xing, J., Wu, Y., Hao, J. Four-
478 Month Changes in Air Quality during and after the COVID-19 Lockdown in Six Megacities
479 in China. *Environ. Sci. Technol. Lett.*, 7, 802-808, 10.1021/acs.estlett.0c00605, 2020c.
- 480 Wang, Y., Wu, G., Deng, L., Tang, Z., Wang, K., Sun, W., Shangguan, Z. Prediction of aboveground
481 grassland biomass on the Loess Plateau, China, using a random forest algorithm. *Sci. Rep.*,
482 7, 6940, 10.1038/s41598-017-07197-6, 2017b.
- 483 Xing, J., Zheng, S., Ding, D., Kelly, J.T., Wang, S., Li, S., Qin, T., Ma, M., Dong, Z., Jang, C., Zhu,
484 Y., Zheng, H., Ren, L., Liu, T.-Y., Hao, J. Deep Learning for Prediction of the Air Quality
485 Response to Emission Changes. *Environ. Sci. Technol.*, 54, 8589-8600,
486 10.1021/acs.est.0c02923, 2020.
- 487 Xue, L.K., Wang, T., Gao, J., Ding, A.J., Zhou, X.H., Blake, D.R., Wang, X.F., Saunders, S.M., Fan,
488 S.J., Zuo, H.C., Zhang, Q.Z., Wang, W.X. Ground-level ozone in four Chinese cities:
489 precursors, regional transport and heterogeneous processes. *Atmos. Chem. Phys.*, 14,
490 13175-13188, 10.5194/acp-14-13175-2014, 2014.
- 491 Yang, J., Wen, Y., Wang, Y., Zhang, S., Pinto, J.P., Pennington, E.A., Wang, Z., Wu, Y., Sander, S.P.,
492 Jiang, J.H., Hao, J., Yung, Y.L., Seinfeld, J.H. From COVID-19 to future electrification:
493 Assessing traffic impacts on air quality by a machine-learning model. *P. Natl. Acad. Sci.*
494 *USA*, 118, e2102705118, 10.1073/pnas.2102705118, 2021a.
- 495 Yang, L., Yuan, Z., Luo, H., Wang, Y., Xu, Y., Duan, Y., Fu, Q. Identification of long-term evolution
496 of ozone sensitivity to precursors based on two-dimensional mutual verification. *Sci. Total*
497 *Environ.*, 760, 143401, <https://doi.org/10.1016/j.scitotenv.2020.143401>, 2021b.
- 498 Yu, S. Fog geoengineering to abate local ozone pollution at ground level by enhancing air moisture.
499 *Environ. Chem. Lett.*, 17, 565-580, 10.1007/s10311-018-0809-5, 2019.
- 500 Yuan, B., Hu, W.W., Shao, M., Wang, M., Chen, W.T., Lu, S.H., Zeng, L.M., Hu, M. VOC emissions,
501 evolutions and contributions to SOA formation at a receptor site in eastern China. *Atmos.*
502 *Chem. Phys.*, 13, 8815-8832, 10.5194/acp-13-8815-2013, 2013.



- 503 Zhan, J., Feng, Z., Liu, P., He, X., He, Z., Chen, T., Wang, Y., He, H., Mu, Y., Liu, Y. Ozone and
504 SOA formation potential based on photochemical loss of VOCs during the Beijing summer.
505 Environ. Pollut., 285, 117444, <https://doi.org/10.1016/j.envpol.2021.117444>, 2021.
- 506 Zhang, X., Li, H., Wang, X., Zhang, Y., Bi, F., Wu, Z., Liu, Y., Zhang, H., Gao, R., Xue, L., Zhang,
507 Q., Chen, Y., Chai, F., Wang, W. Heavy ozone pollution episodes in urban Beijing during
508 the early summertime from 2014 to 2017: Implications for control strategy. Environ. Pollut.,
509 285, 117162, <https://doi.org/10.1016/j.envpol.2021.117162>, 2021.
- 510 Zhao, H., Chen, K., Liu, Z., Zhang, Y., Shao, T., Zhang, H. Coordinated control of PM_{2.5} and O₃ is
511 urgently needed in China after implementation of the “Air pollution prevention and control
512 action plan”. Chemosphere, 270, 129441,
513 <https://doi.org/10.1016/j.chemosphere.2020.129441>, 2021.
514